V2b neurons act via multiple targets in spinal motor networks

Mohini Sengupta[1] and Martha W. Bagnall[1]

[1]Washington University School of Medicine, Department of Neuroscience, St Louis, MO, USA.

Corresponding author:

Martha W. Bagnall

bagnall@wustl.edu

Word count: 5097 words. Figures: 7

Acknowledgments:

This research was funded by the Pew Scholar Award (M.W.B), R01 DC016413 (M.W.B), a McKnight Scholar Award (M.W.B.), and the McDonnell Center for Cellular and Molecular Neurobiology Postdoctoral Fellowship 2021 (M.S.).

Abstract

Local neurons within the spinal cord guide activity of specific motor neurons and muscles for execution of different movements. These interneuron populations also interact with each other to critically influence motor output, but a systematic mapping of their connectivity has not been performed. This is especially true for connectivity in the rostrocaudal axis, along which most interneurons project long-range axons. In this study, using larval zebrafish, we mapped local and long-range connectivity of a cardinal spinal population, V2b neurons. Gata3^{+} V2b neurons send ipsilateral, descending neurons that inhibit their postsynaptic targets. We show that V2b neurons are active during fictive swimming, providing on cycle inhibition that mostly leads the motor burst. In addition to motor neurons, V2bs inhibit other prominent interneuron classes including V2a, V1 and other V2b neurons, but neither of two categories of dorsal horn sensory neurons. Furthermore, V2b inhibition exhibited a distinct pattern of contacts along the R-C axis, providing long-range inhibition to motor neurons and V2as but more localized innervation of inhibitory V1s. Together, these results demonstrate that V2b connectivity varies along the rostrocaudal axis according to the identity of its synaptic target. Furthermore, in conjunction with prior work, these results provide the first demonstration of reciprocal V1/V2b inhibition in axial circuits, potentially providing an ancestral template of the limb control network.

Introduction

In vertebrates, locomotor movements are executed by intrinsic networks in the spinal cord[1–3]. Spinal networks comprise excitatory and inhibitory interneurons that connect with each other and with motor neurons to orchestrate different movements[3,4]. Across vertebrates, neuronal genetic identity, morphology, and neurotransmitter expression remain remarkably conserved, making it convenient to study and apply knowledge across species[3,5]. Behaviorally, coordination along the rostro-caudal axis during locomotion is also a conserved feature[6–9], yet mechanisms that facilitate this coordination are not completely understood. A primary reason for this gap is the lack of knowledge on long range connectivity of neurons. In our previous work, we revealed that spinal V1 neurons inhibited different post-synaptic targets locally and distally, implying significant variations in longitudinal connectivity and function[10]. An equivalent analysis of rostro-caudal organization of connectivity remains to be performed for other spinal populations.

Spinal V2b neurons are a prominent, inhibitory population marked by expression of the Gata3 transcription factor across vertebrates[11–13]. In mice[14] and zebrafish[13], V2b neurons project ipsilateral descending axons spanning several segments, but apart from contacting motor neurons and other V2bs[13], V2b postsynaptic partners are unknown. In mice, V2b neurons have been identified as a subset of Long Descending Propriospinal Neurons (LDPNs) that connect cervical and lumbar segments[14] and are thought to implement inter-limb coordination during locomotion[15]. How V2b neurons achieve this is not known.

Functionally, V2bs have primarily been implicated in limb movements, where together with V1 neurons, they enforce flexor-extensor alternation[16,17]. However, V2b neurons are present not only in spinal segments that control limb motor neurons but all along the spinal cord in both mice[18] and zebrafish[13], suggesting an ancestral role in locomotor coordination. In these axial circuits, some evidence suggests V2b neurons can serve as locomotor brakes[13]. Bilateral optogenetic activation of V2b neurons in spinally transected zebrafish reduced frequency of tail movements, whereas suppression of V2b neurons led to accelerated swimming.

In this study, we analyzed recruitment pattern and longitudinal connectivity of V2b neurons in axial motor networks of larval zebrafish. We show that V2b neurons are active during swims with phase lead in the swim cycle. Via circuit mapping, we demonstrate that V2b neurons inhibit motor neurons as well as other cardinal excitatory and inhibitory spinal populations, including V1 neurons. Moreover, V2b inhibition is structured in a specific pattern in the R-C axis. Combined, these results indicate that V2b neurons have a multifaceted role in axial motor control that may have provided a template for limb control circuits.

Materials and Methods

Animals: Adult zebrafish (Danio rerio) were maintained at 28.5°C with a 14:10 light:dark cycle in the Washington University Zebrafish Facility following standard care procedures. Larval zebrafish, 4–6 days post fertilization (dpf), were used for experiments and kept in petri dishes in system water or housed with system water flow. Animals older than 5 dpf were fed rotifers or

Gemma dry food daily. All procedures described in this work adhere to NIH guidelines and received approval by the Washington University Institutional Animal Care and Use Committee.

Transgenic Fish Lines: For recruitment studies in Figure 1, V2b neurons were targeted in the stable *Tg (Gata3:LoxP-dsRed-LoxP:GFP) nns53Tg* (ZDB-ALT-190724-4)[13]. For all connectivity experiments, the stable transgenic line *Tg(Gata3:Gal4;UAS:CatCh) stl602* (DB-ALT-201209-12)[13] generated by Tol2 mediated transgenesis previously in our lab was used. For targeting V2a and V1 neurons, the *Tg(vsx2:loxP-DsRed-loxP-GFP) nns3Tg* (ZDB-ALT-061204-4)[19] and *Tg(En1: LoxP-dsRed-LoxP:DTA) nns55Tg* (ZDB-ALT-191030-2)[20] lines, respectively, were crossed to *Tg(Gata3:Gal4;UAS:CatCh)* to generate double transgenics. Secondary motor neurons were targeted in part using the *Tg(mnx:pTagRFP) stl603* line created in the lab.

Electrophysiology: 4–6 dpf larvae were immobilized with 0.1% α-bungarotoxin and fixed to a Sylgard lined petri dish with custom-sharpened tungsten pins. One muscle segment overlaying the spinal cord was removed at the mid-body level (segments 9–13). The larva was then transferred to a microscope (Nikon Eclipse E600FN) equipped with epifluorescence and immersion objectives (60X, 1.0 NA). The bath solution consisted of (in mM): 134 NaCl, 2.9 KCl, 1.2 $MgCl_2$, 10 HEPES, 10 glucose, 2.1 $CaCl_2$. Osmolarity was adjusted to ~295 mOsm and pH to 7.5. For recording V2b spiking during swims, a combination of cell attached and whole cell patch clamp recordings were obtained from V2b neurons. Patch pipettes (7–15 MΩ) were either filled with extracellular saline (cell attached) or patch internal (whole cell) solution and targeted to a V2b neuron. After formation of a gigaohm seal, extracellular spikes were recorded in cell attached mode. To obtain whole cell recordings, brief suction pulses were used to break into the cell. Spiking was recorded in current clamp mode using the following patch internal solution: (in mM) 125 K gluconate, 2 $MgCl_2$, 4 KCl, 10 HEPES, 10 EGTA, and 4 Na_2ATP. Ventral root recordings were obtained 2-3 segments caudal to the recorded V2b, using suction electrodes (diameters 20-50 µm). Fictive swimming (~20-50 Hz) was elicited by either a brief electric stimulus to the tip of the tail (10-20 V for 0.2-1 ms)[20] or a visual stimulus of blue and white moving gratings (spatial width 1cm at a speed of 1cm/s)[21].

For mapping connectivity to target neurons, larvae were immobilized and dissected as before. Whole cell patch clamp recordings were made from target neurons in voltage clamp mode using the following patch internal solution: (in mM) 122 cesium methanesulfonate, 1 tetraethylammonium-Cl, 3 $MgCl_2$, 1 QX-314 Cl, 10 HEPES, 10 EGTA, and 4 Na_2ATP. APV (10 µM) and NBQX (10 µM) were added to the bath to block glutamatergic transmission. For all patch internal solutions, pH was adjusted to 7.5 and osmolarity to 290 mOsm. Additionally, for whole cell recordings, sulforhodamine 0.02% was included in the patch internal to visualize morphology of recorded cells post-hoc. Recordings were acquired using a Multiclamp 700B amplifier and Digidata 1550 (Molecular Devices). Signals were filtered at 2 kHz and digitized at 100 or 50 kHz. For IPSCs, cells were recorded at +0.3 mV (after correction for liquid junction potential of 14.7 mV).

Optogenetic Stimulation: A Polygon 400 or 1000 Digital Micromirror Device (Mightex) was used to deliver optical stimulation. The projected optical pattern consisted of a 4x4 grid of 16 squares. Each square in the grid approximately measured 20µm x 20µm and covered 0-6 cells depending on position. One full stimulus pattern consisted of an ordered sequence of turning ON and OFF each of the 16 squares sequentially. For each small square, illumination consisted of a 20 ms light pulse (470 nm) at 50% intensity (4.6-5.2 µW under 60X, 1.0 NA). The sequence was triggered using a TTL pulse from the Digidata to synchronize the stimulation with

electrophysiology. The objective was carefully positioned over a single spinal segment prior to stimulus delivery; for each new segment, the stage was manually translated and repositioned. V2b spiking reliability was measured by delivering multiple trials to a selected square that had evoked spiking on the first trial. A similar protocol was used for all segments to obtain reliable IPSCs for measurement of conductances. For the high frequency stimulation in Fig. 3, a single square was illuminated with a 20 Hz train of five 20 ms pulses.

Analysis: Electrophysiology data were imported into Igor Pro 6.37 (Wavemetrics) using NeuroMatic[22]. Spikes and IPSCs were analyzed using custom code in Igor and MATLAB. For analyzing motor recordings from the ventral nerve (Fig 1), the raw swim signal (Fig. 1B, grey traces) was converted to the standard deviation signal over a sliding window of 10 ms (Fig. 1B, blue traces). Peaks from this SD signal (corresponding to the midpoint of motor bouts) were calculated using custom written MATLAB codes and used for all subsequent analysis. For measurement of spike timing relative to phase, V2b spikes occurring between two motor bursts were selected and the time difference of V2b spike from first motor was divided with the time difference between the motor bursts. Histograms of these spike times were normalized for each cell and then pooled together (from 12 cells) for the summary plot shown in Fig. 1C. For connectivity experiments (Fig 3-7), data were analyzed as previously reported[10]. Briefly, charge transfer for the evoked response was calculated by integrating the current in a 50 ms window from the onset of the optical stimulus (Evoked) and subtracting this from Control 1, a similar integral over a 50 ms window before the optical stimulus. This was done to account for spontaneous activity. To calculate background noise values, a similar integral for a different 50 ms window at the end of the recording (Control 2) was subtracted from Control 1. Both the charge transfer of the evoked response and background noise were summed across the 16 squares for each segment.

$$Charge\ transfer(Segment\ i, square\ j) = Evoked(i,j) - Control\ 1(i,j)$$
$$Noise(Segment\ i, square\ j) = Control\ 2(i,j) - Control\ 1(i,j)$$
$$Total\ evoked\ charge\ transfer\ (Seg\ i) = \sum_{j=1}^{16} Charge\ transfer(i,j)$$
$$Total\ noise\ (Seg\ i) = \sum_{j=1}^{16} Noise\ (i,j)$$

For statistical comparisons, *Total evoked charge transfer (Seg i)* was compared to *Total noise (Seg i)* for each target population using the Wilcoxon Sign Rank Test ($p<0.05$). Statistical tests were performed using MATLAB (R2020b, MathWorks). Due to the non-normal distribution of physiological results, including spiking and IPSC charge transfer, we chose to use nonparametric statistics and tests for representations and comparisons.

Peak amplitudes of IPSCs were calculated from the first IPSC only to avoid effects from synaptic depression/facilitation. Conductances were calculated from peak amplitude / driving force (75 mV). Input resistance was measured by an average of small hyperpolarizing pulses.

Results

V2b activity during fictive swimming

Spinal interneurons in the ventral horn that participate in generating rhythm or pattern of motor activity show stereotypic firing patterns during movements[20,23,24]. Therefore, studying these

patterns, especially the temporal profile of activity can provide crucial insight into their recruitment and functions. To study firing patterns of V2b neurons, we recorded from identified neurons in the transgenic *Tg(Gata3:lox-dsred-lox:GFP)* line while simultaneously monitoring fictive motor activity from ventral nerve responses in paralyzed zebrafish larvae at 4-6 dpf (Fig. 1A). Fictive swims (20-50 Hz) were evoked either by a brief electric shock to the tail or a visual stimulus of moving bars. Over half of V2b neurons (20 out of 32 recorded, 62.5%) did not exhibit any spiking during fictive swims. Among V2b neurons that did fire during motor episodes, spiking rates were similar between cell attached (Fig. 1B, left) and whole cell (Fig. 1B, right) recordings and hence were pooled for subsequent analysis. To investigate if V2b spiking was phase locked relative to the swim cycle, we constructed histograms of V2b spike times normalized with respect to the phase of motor activity. The population data is summarized in Fig. 1C (N=12 neurons). Because V2b neurons are ipsilateral and inhibitory, we expected them to provide on cycle inhibition, peaking close to 0 or 1. Instead, the highest frequency was centered at a phase value of 0.85 implying that most V2b inhibition coincides with the rising phase of on cycle excitation and motor neuron spiking. This is also evident from representative traces in Fig. 1B. V2b neurons do not exhibit a tight phase coupling: individual neurons displayed different phase values, resulting in a wide distribution. This suggests that V2b neurons form a functionally heterogenous group. Such coincident inhibition can have different consequences on motor activity depending on the post synaptic target. Therefore, next, we decided to map post synaptic partners of V2b neurons.

Optogenetic assisted mapping of V2b connectivity

Spinal neurons exhibit high diversity. At least eight cardinal classes in the ventral horn and several similar populations in the dorsal horn have been identified[3,4]. To map V2b connectivity along the rostrocaudal axis, we utilized the high throughput technique of optogenetic assisted circuit mapping[25]. We used the transgenic line *Tg(Gata3:Gal4;UAS:CatCh)*, in which V2b neurons expressed a calcium permeable variant of Channelrhodopsin, CatCh[26] (Fig. 2A, schematic). We first calibrated the efficacy and specificity of the optical stimulus for activating V2b neurons restricted to a single segment. A 4x4 square grid pattern was projected approximately over a single spinal segment (Fig. 2B). Each square in this grid measured 20x20 μm^2 in area, covered approximately 4-6 $CatCh^+$ neurons depending on expression and was illuminated in a sequential order with a square, 20 ms light pulse at 50% power. V2b neurons recorded in current clamp mode exhibited a mean resting membrane potential of -74.3 ± 2.37 mV. When directly illuminated on the soma (black dot) or nearby, V2b neurons exhibited robust spiking (Fig. 2C, red traces). V2b neurons send descending axons in the R-C axis, extending up to seven segments[13]. To map connectivity in this axis, it is imperative that the optical stimulus does not elicit antidromic spikes when the axon is illuminated. To test this, we translated an identical grid optical stimulus to neighboring segments in both the rostral and caudal directions while recording V2b somatic responses (Fig. 2D). Optical stimulation outside of Segment 0 (segment in which V2b is being recorded) did not evoke any appreciable activity (Fig. 2D, E,

N=10 neurons). We also tested reliability of V2b spiking with repeated trials of the optical stimulus. V2b neurons showed high reliability of spiking with a mean reliability of 75% ± 12.1 (Fig. 2F, N=10 neurons). Together, these data show that the grid optical stimulus activated V2b neurons in a spatially restricted manner and therefore can be utilized next for mapping V2b connectivity to different targets along the R-C axis.

V2b neurons robustly inhibit motor neurons up to long distances

In mice, V2b neurons in lumbar segments make anatomical contacts to motor neurons, preferentially those controlling extensors[16]. In larval zebrafish, physiological studies show that V2b neurons inhibit both fast, primary motor neurons and slow, secondary motor neurons[13], but it is not known if this connectivity is only local or extends to distal segments. To investigate this, we recorded intracellularly from primary motor neurons in the previously calibrated *Tg(Gata3:Gal4;UAS:CatCh)* line (Fig. 3A). Primary motor neurons were identified in bright field with their characteristic large, laterally positioned soma and post hoc dye fill showing extensive muscle innervation[27]. Cells were recorded using a cesium internal, held at 0 mV and bathed in glutamate receptor blockers (NBQX, APV) to isolate inhibitory post synaptic currents (IPSCs). The grid optical stimulus was delivered at a single segment each time and then moved rostrally for 7 segments to cover the full descending axon length of V2b neurons.

Primary motor neurons recorded in this configuration exhibited IPSCs when V2b neurons were optically activated both nearby (Fig. 3B, Seg 1) and at long range (Fig. 3B, Seg 7). To quantify these inputs, we calculated the charge transfer of evoked IPSCs (Fig. 3B, inset) for each segment and compared it to noise (See Methods). As shown in Fig. 3B (lower panel), primary motor neurons received significant V2b inhibition even up to seven segments away (N=25 neurons; Wilcoxon Sign Rank Test, $p < 0.01$). We next performed similar mapping from V2b neurons to secondary motor neurons. These were targeted through a mixture of gene expression in the double transgenic *Tg(Gata3:Gal4;UAS:CatCh ; mnx:ptag:RFP)* line and post hoc dye label. Secondary motor neurons also received local and long-range inhibition from V2bs (Fig. 3C). Charge transfer at Segments 1 through 5 were significantly above noise levels (Fig. 3C, lower panel, N=11 neurons; Wilcoxon Sign Rank Test, $p < 0.01$) but dropped at Segment 7.

V2b neurons in zebrafish have purely descending axons, and therefore are not expected to inhibit neurons in the rostral direction. Consistent with this expectation, we saw little to no evoked IPSCs during delivery of optical stimuli caudal to the recorded segment (Segments -1, -2) (Fig. 3B, C). Because our transgenic line also labels CSF-cNs (Fig. 2B, grey arrowheads) which send purely ascending axons[28,29] and are known to selectively inhibit CaP motor neurons[30], this low-amplitude connectivity likely results from activation of CSF-cNs.

To verify that evoked IPSCs were monosynaptically generated, we delivered a train of optical stimuli (five 20 ms pulses at 20Hz). IPSCs followed the train with consistent latency and low jitter, consistent with monosynaptic connectivity (Fig. 3D).

Finally, we asked if V2b connectivity to motor neurons showed differences in number and/or strength of connections with distance. As a proxy for number of connections, we quantified the fraction of small squares in the 4x4 grid stimulus in each segment that successfully evoked IPSCs. Both primary and secondary motor neurons did not show any differences in the number of V2b connections along the longitudinal axis (Fig. 3E, N=16 pMNs and 11 sMNs; Kruskal Wallis Test and post hoc Tukey's test, $p > 0.01$). To quantify IPSC strength, we repeatedly stimulated a single square of the optical stimulus to reliably evoke IPSCs and measured peak amplitudes. Primary and secondary motor neurons did not show any significant change in strength of V2b inputs along the longitudinal axis (Fig. 3F, N=16 pMNs, N=8 sMNs; Kruskal Wallis Test and post hoc Tukey's test, $p > 0.01$), however, for sMNs, IPSCs were less reliably evoked at Segment 7 and hence were not included. Taken together, these data show that V2b neurons monosynaptically inhibit both primary and secondary motor neurons locally and at long distances. V2b inhibition extends longer for primary motor neurons than secondary motor neurons, maintaining a steady number and strength of connections along the R-C axis.

V2b neurons inhibit excitatory V2a neurons at long range

Spinal V2a neurons are a major source of excitatory drive to motor neurons[31–35]. These neurons participate in rhythm generation and are indispensable for motor functions[34,36]. Therefore, we next sought to investigate V2b-mediated inhibition of the V2a population along the longitudinal axis. V2a neurons were targeted using the *Tg(Chx10:lox-dsred-lox:GFP)* line that was crossed to *Tg(Gata3:Gal4;UAS:CatCh)* as shown in Fig. 4A. As with motor neurons, V2a neurons also received inhibitory synaptic inputs from V2b neurons in both local and distal segments (Fig. 4B). Charge transfer of inhibitory currents was significantly higher than noise for up to seven segments from the recording site (Fig. 4C, N=10 neurons; Wilcoxon Sign Rank Test, $p < 0.01$). V2a neurons did not receive any appreciable evoked synaptic input when caudal segments were illuminated (Fig. 4C, Segment -1, -2). As in primary motor neurons, the inferred number and strength of V2b inhibitory inputs remained high along the rostrocaudal axis (Figure 4D, E) (N=8 neurons; Kruskal Wallis Test and post hoc Tukey's test, $p > 0.01$). Overall, these data reveal that V2b neurons inhibit V2a neurons locally and long-range, identifying the V2a population as a novel target of V2b inhibition.

V2b neurons inhibit spinal V1 neurons locally

V1 neurons are a major inhibitory population in the spinal cord[37–39] and share a special relationship with V2bs for limb control[16]. In lumbar networks that control the hind limbs, V1/V2b neurons are known to reciprocally inhibit antagonistic motor pools allowing alternation of flexors and extensor for limb movements. Flexor-extensor related Ia inhibitory interneurons have been shown to directly inhibit each other in several species[24,40,41], including humans[42]. While Ia inhibitory neurons belong to the V1/V2b populations[43], direct evidence of reciprocal inhibition between these two genetically defined populations has not been found. To determine if V2b neurons inhibit the V1 population, we next recorded from V1 neurons using the

Tg(eng1b:lox-dsred-lox:DTA) line (Fig. 5A). As shown in Fig. 5B, V1 neurons received evoked IPSCs locally, at Segments 1 and 3, but to our surprise, not distally at Segment 7. This pattern was in contrast to the long-range V2b inhibition onto motor neuron and V2a targets. Charge transfer for evoked IPSCs was significantly different from noise at Segments 0-3 (Fig. 5C, N= 9 neurons; Wilcoxon Sign Rank Test, $p < 0.01$) but not at long ranges, Segments 5 and 7. The number of V2b connections decreased along the R-C axis (Fig. 5E, N=9 neurons; Kruskal Wallis Test and post hoc Tukey's test, $p<0.01$), suggesting lesser number of V2b neurons made functional contact with V1s at long ranges. Within the nearby segments in which V1 neurons were inhibited (0-3 segments), the strength of V2b IPSCs was consistent (Fig. 5F, N=9 neurons; Kruskal Wallis Test and post hoc Tukey's test, $p>0.01$). Therefore, the structure of V2b-mediated inhibition varies along the longitudinal axis to distinct downstream targets and for the first time, we demonstrate direct connectivity of V2b neurons to the V1 population.

V2b connectivity to other ventral spinal populations

We next extended this map to include other spinal populations in the ventral horn. Commissural neurons in the spinal cord are a major functionally relevant group that helps secure left-right alternation[44–46], rostro-caudal coordination[15,23], and modulation of motor strength[47,48]. Commissural neurons comprise more than one genetically defined class (dI6, V0v, V0d and V3 neurons[45,49–52]), and also exhibit morphological variability within each class. To first determine whether V2bs target any commissural neuron, we performed blind recordings of neurons and classified them post hoc based on their morphology from dye fills as commissural, bifurcating and ascending neurons, likely belonging to the V0/dI6 classes. We collectively refer to these as Commissural Premotor neurons or CoPrs. CoPr neurons were located more dorsally than the described locus of V3 neurons and therefore are unlikely to be included in this population. CoPr neurons received minimal inputs from V2b neurons (Fig. 6A, middle), significant only at Segment 0 (Fig. 6A, N= 7 neurons; Wilcoxon Sign Rank Test, $p < 0.01$) and absent at longer distances. These results suggest that V2b neurons predominantly target ipsilateral pathways.

V2b neurons have been shown to inhibit each other[13], but the rostrocaudal extent and amplitude of this inhibition is unknown. We observed V2b inhibition onto other V2b neurons locally (Fig. 6B, N= 9 neurons; Wilcoxon Sign Rank Test, $p < 0.01$) but not at long range.

V2b neurons do not inhibit two dorsal horn sensory populations

Finally, we wanted to test if V2b neurons exhibited any prominent sensory targets. In zebrafish, the Commissural Primary Ascending (CoPA) neurons, likely homologous to mammalian dI5 neurons, are glutamatergic neurons activated during the tactile reflex[53]. During swims, CoPAs are gated by V1 neurons[10,37] and possibly others[53]. CoPA neurons are readily identifiable by their distinct axonal and dendritic morphology in posthoc dye fills. Fig. 6C shows representative traces (middle) and summary data (bottom) of V2b inputs to CoPA neurons. CoPAs did not receive any appreciable inhibition from V2b neurons (N= 12 neurons; Wilcoxon Sign Rank Test, $p > 0.01$) suggesting that V2bs are not involved in sensory gating of CoPA neurons during

swims. Interestingly, CSF-cNs are known to contact CoPAs[30]. However, we did not capture this connection, even in the caudal segments (Fig. 6C, Segments -1, -2), probably because our optical stimulus did not reliably activate CSF-cNs. We also examined responses in Dorsal Longitudinal (DoLA) neurons, a sensory target likely homologous to mammalian dI4 neurons. DoLAs are GABAergic and exhibit a characteristic axonal morphology but much less is known about their function. As shown in Fig. 6D, V2b neurons did not show any appreciable inputs to DoLA neurons (N= 3 neurons; Wilcoxon Sign Rank Test, $p > 0.01$). These experiments show that inhibition of these sensory targets is not a primary function for V2b neurons.

To collate our results of V2b connectivity to different cell types, we plotted a heat map showing median charge transfer for each population across the R-C axis (Fig. 7). For each population, charge transfer for each cell was first normalized to its total cellular conductance (inverse of input resistance) to allow a direct comparison of the effect of V2b inhibition across targets. This map clearly reveals three key results: (i) V2b output is primarily focused on motor and premotor targets in the ventral horn; (ii) Within the ventral horn, V2b inhibition is selective, aimed at motor neurons, V2a and V1 neurons but not significantly at commissural populations; and (iii) V2b inhibition is spatially structured along the rostrocaudal axis, exhibiting different synaptic partners locally and at long ranges.

Discussion

In this study we show for the first time that V2b neurons are active largely both in phase and leading the swim cycle, with heterogeneity across the population. V2b neurons inhibit motor neurons and major ventral horn spinal populations, including V1 and V2a neurons. In contrast, they do not inhibit two populations of dorsal horn sensory neurons, suggesting they have a predominantly motor role. Furthermore, V2b inhibition shows a selective spatial organization in the rostrocaudal axis, supplying long range inhibition to motor neurons and V2as but local connectivity to inhibitory V1 neurons, setting up a local disinhibitory circuit. In conjunction with previous work, this pattern of synaptic output indicates that axial V1 and V2b populations reciprocally inhibit each other with a rostrocaudal structure, similar to the inferred circuit for limb control in later vertebrates.

Coincident inhibition to motor neurons

Traditionally, spinal inhibition is conceptualized as alternating with inhibition, setting up oscillations that drive rhythmic movements[54]. Recent studies, however, have shown another form of inhibition in motor neurons that is coincident with excitation[55,56]. The source of this coincident inhibition or its significance to motor control remain unknown. Our results showing high frequency of V2b spiking at phase values of 0.8-0.9 indicating that V2bs supply one source of coincident inhibition to motor neurons. Such coincident inhibition is widespread in the cerebral cortex where it regulates network parameters like synaptic gain through input normalization, dynamic range and spike synchrony[57]. Gain modulation by inhibitory conductances have been shown in motor neurons but the source of inhibition is not known[58,59]. Interestingly, V2b neurons are not the only source of on cycle inhibition. V1 neurons also provide on cycle inhibition[20], but

the timing of V1 spiking is substantially shifted compared to V2b activity. During the swim cycle, V1 firing peaks at phase values of 0-0.1, indicating V1 neurons are active after the start of the motor burst. This phase relation is well suited to the known function of V1 neurons, motor burst termination permitting fast speeds of locomotion[20,38]. V2b neuron spiking, on the other hand, precedes the motor burst, coinciding with the rising phase of excitation. Given this temporal profile, V2bs are well poised for adjusting the gain of target neurons. Future experiments investigating effect of V2b inhibition on motor neurons during swims will help shed light on the importance of timing of V2b spiking.

Long-range inhibition of motor neurons and V2a neurons

Locomotion requires efficient coordination along the rostro-caudal axis. In aquatic vertebrates, this takes the form of an S-shaped body during swimming, with a complete activity cycle from rostral to caudal[6]. Similarly, in limbed animals, the left forelimb and right hind limb are synchronously active during most locomotion. Such coupling is mediated by spinal intrinsic networks as it is observed in isolated spinal cord preparations[60], but what neurons or mechanisms enforce this coordination are not completely known. Recent studies indicate that commissural excitatory neurons, the V0v population, play a key role through long range activation of contralateral motor neurons[15,23]. As observed for other aspects of motor control like speed regulation, along with selective excitation, active inhibition of specific targets is also necessary to enforce motor rhythms/patterns[20,61]. Therefore, for diagonal coordination to work efficiently, long range inhibition in the ipsilateral axis is a crucial requirement, as shown in modeling studies of inter-limb coordination[62]. Our results showing that V2b neurons inhibit motor neurons at long distances provide a potential mechanism for enforcing ipsilateral inhibition in the R-C axis to facilitate diagonal coupling. Moreover, by also inhibiting V2a neurons, the primary excitatory drive to motor neurons, over long distances, V2bs might reinforce rostrocaudal propagation. Consistent with this function of V2b neurons is our observation that V2bs do not appreciably inhibit commissural neurons, especially at long distances. This proposed role of V2b inhibition is also supported in studies in mice, where V2b neurons have been identified as part of Long Descending Propriospinal neurons (LDPNs)[14] that have been shown to facilitate interlimb coordination[15,63]. Direct behavioral testing of rostrocaudal coordination in V2b ablated animals will be required to tease out the effects of long range V2b inhibition.

Local reciprocal inhibition of V1 neurons

Combined with our previous results on V1 connectivity[10], we show that V1 and V2b neurons reciprocally inhibit each other. This circuit motif resembles reciprocal inhibition for flexor-extensor modules in the following ways: 1) Mutual inhibition between Ia inhibitory interneurons has been reported in several species[24,40–42] and thought to be a crucial component for enforcing flexor-extensor alternation[54]. Though it is known that Ia inhibitory interneurons belong to the V1/V2b populations, V1/V2b reciprocal innervation has so far not been systematically analyzed. 2) In our results, both V1 and V2b neurons inhibit each other locally, up to three segments away. Given that V2bs project descending axons and V1s send axons in the ascending direction, V1/V2b reciprocal connectivity also has a rostrocaudal attribute. This is consistent with the rostrocaudal and local structure of flexor-extensor circuits[65], where the predominant flexor motor

neuron signal is at L2 (Lumbar 2), three segments rostral to the predominant extensor motor neuron signal at L5[16]. The origin of limb networks is debated. Some evidence suggests that tetrapod locomotion evolved from undulatory swimming and hence networks for limb control originated through gradual modification of circuits regulating axial musculature[5,64,66,68]. Our results showing V1/V2b reciprocally inhibitory circuits in axial networks may therefore provide evidence of an ancestral circuit motif that could have been co-opted for flexor-extensor control.

The functional relevance of V1/V2b reciprocal connectivity in axial motor control is still not clear. Interestingly, loss of V1 or V2b neurons in larval zebrafish shows opposing behavioral effects; knock out of V1 neurons slows down locomotion[20] while suppression of V2b neurons yields an increase in locomotor speed[13]. While our connectivity data separately supports these behavioral effects, how V1/V2b reciprocal inhibition fits into this picture remains to be seen. Current analysis of V1/V2b connectivity does not reveal any biases to any speed modules[10]. Future studies with simultaneous recording of V1/V2b activity during different speeds of locomotion will help solve this puzzle. Overall, we show evidence of an ancestral version of V1/V2b reciprocally inhibitory network suggesting that mammalian locomotor strategies indeed have primordial underpinnings.

Current models for generating rhythmic locomotion are often incomplete due to lack of knowledge on activity and connectivity of interneurons. Although clearly observed in motor neurons in several species, coincident inhibition remains excluded in models of rhythmic locomotion. In models for flexor-extensor networks, many interactions among and between groups like Renshaw cells and Ia inhibitory interneurons have been incorporated to implement the motor pattern[54], yet a dearth of direct evidence makes linking these functions to known genetic classes difficult[67]. Similarly, models for inter-limb coordination also require long descending inhibition as a crucial component, yet identity of these projections remain unknown[62]. In this study, by providing a detailed analysis of V2b activity during fictive swims and connectivity to motor neurons and other prominent genetically defined populations, we provide much needed information to fill gaps in current models and enhance our understanding of spinal motor control and its evolution.

Figures:

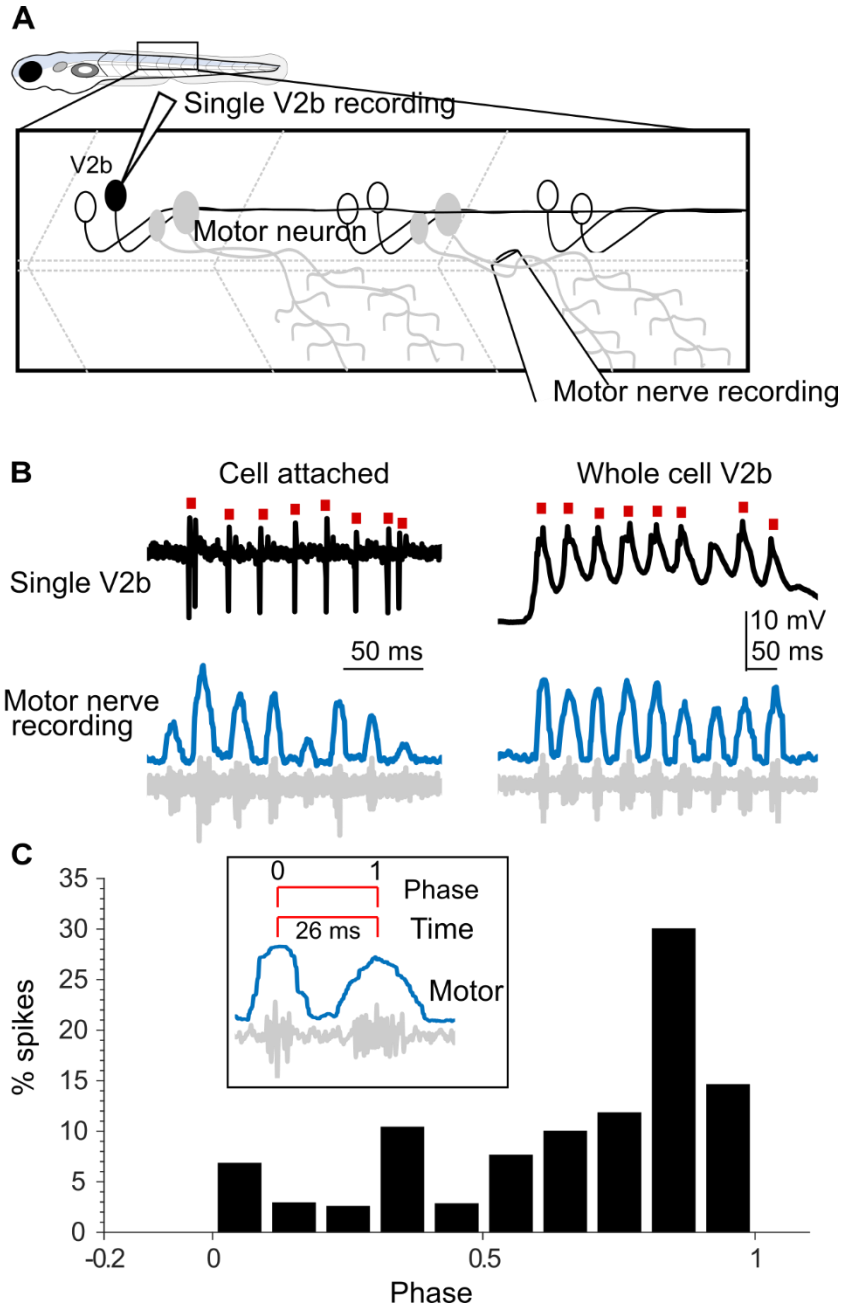

Figure 1: Activity of V2b neurons during fictive swim. A. Schematic of the experimental set-up showing simultaneous intracellular recording from single V2b neurons and extracellular recording of the motor nerve. B. Representative traces showing V2b spikes (top, black) recorded in cell attached (left) or whole cell (right) mode during motor activity (bottom, grey). Red squares mark V2b spikes. The standard deviation over a sliding 10 ms window was used to determine the midpoint of motor bursts (blue trace). C. Histogram of V2b spike timing with respect to normalized phase of motor activity. Inset: Illustration for timing and phase relation between successive motor bouts. N= 686 swim cycles from 12 neurons.

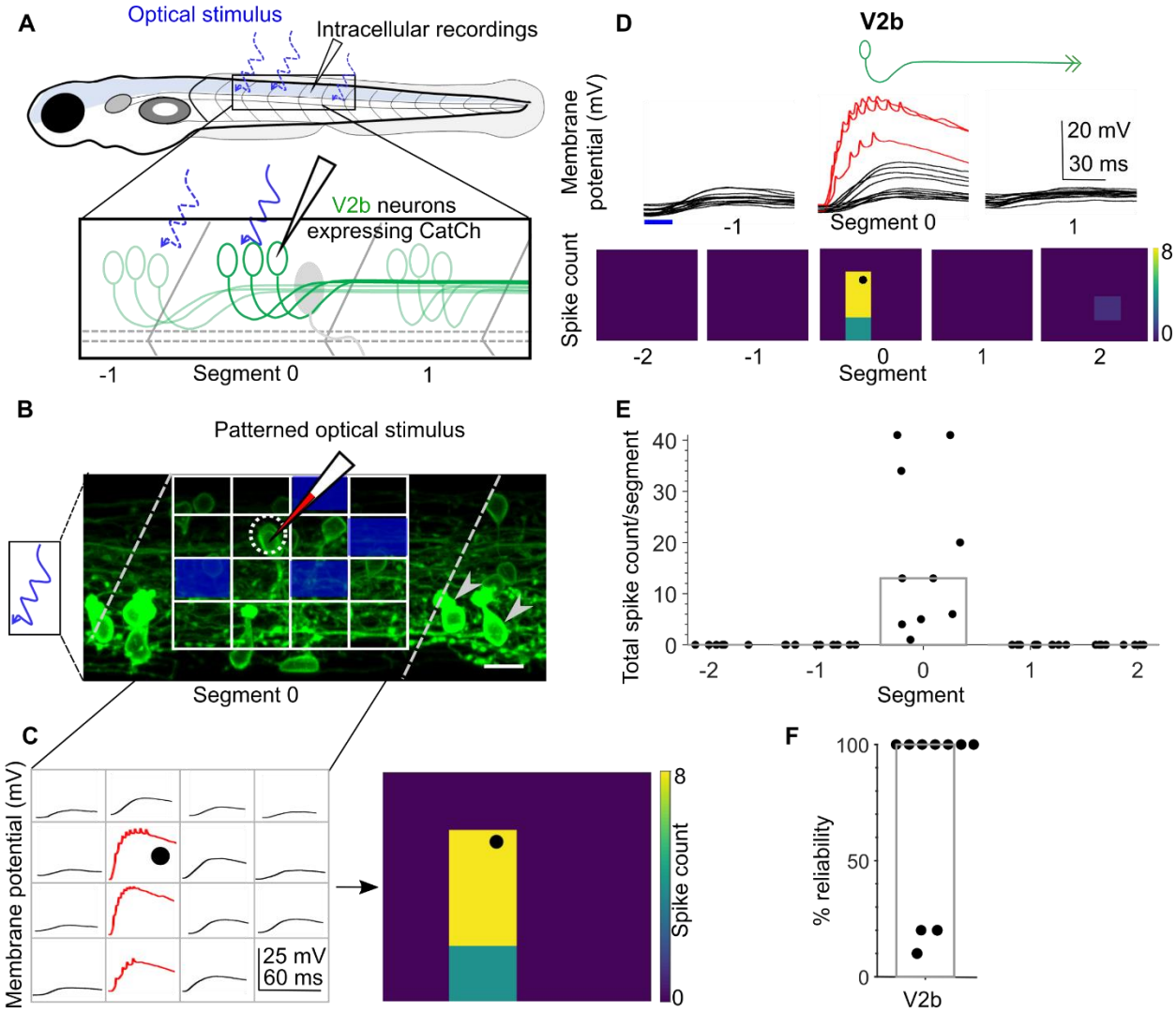

Figure 2: Calibration of V2b activation by patterned optical stimulus. A. Schematic of the experimental set-up showing targeted intracellular recording and optical stimulation in *Tg(Gata3:Gal4,UAS:CatCh)* animals. B. Schematic of the patterned optical stimulus. A 4x4 grid was overlaid on approximately one spinal segment and each small square in the grid (blue square) was optically stimulated in sequence with a 20 ms light pulse at 50% power. Position of the recorded cell is outlined in a grey dotted circle. Arrowheads show CSF-cNs also labeled in this line. C. Intracellular recordings elicited from optical stimulation in each grid square (left). Spiking is denoted in red. Same data shown as a heat map superimposed on the stimulus grid (right). Position of the recorded cell is indicated with a black dot. D. V2b responses evoked by optical stimuli in segments rostral or caudal to the recorded neuron. Representative traces of activity (top) and spike count (bottom) of the same V2b neuron while the optical stimulation was moved along the rostro-caudal axis. Red traces indicate spiking. E. Quantification of spiking in V2b neurons as the optical stimulus is presented along the rostro-caudal axis. N = 10 neurons. Bar indicates median value. F. Reliability of spiking in these neurons with multiple trials of the same optical stimulus. N=10 neurons. Bar indicates median value.

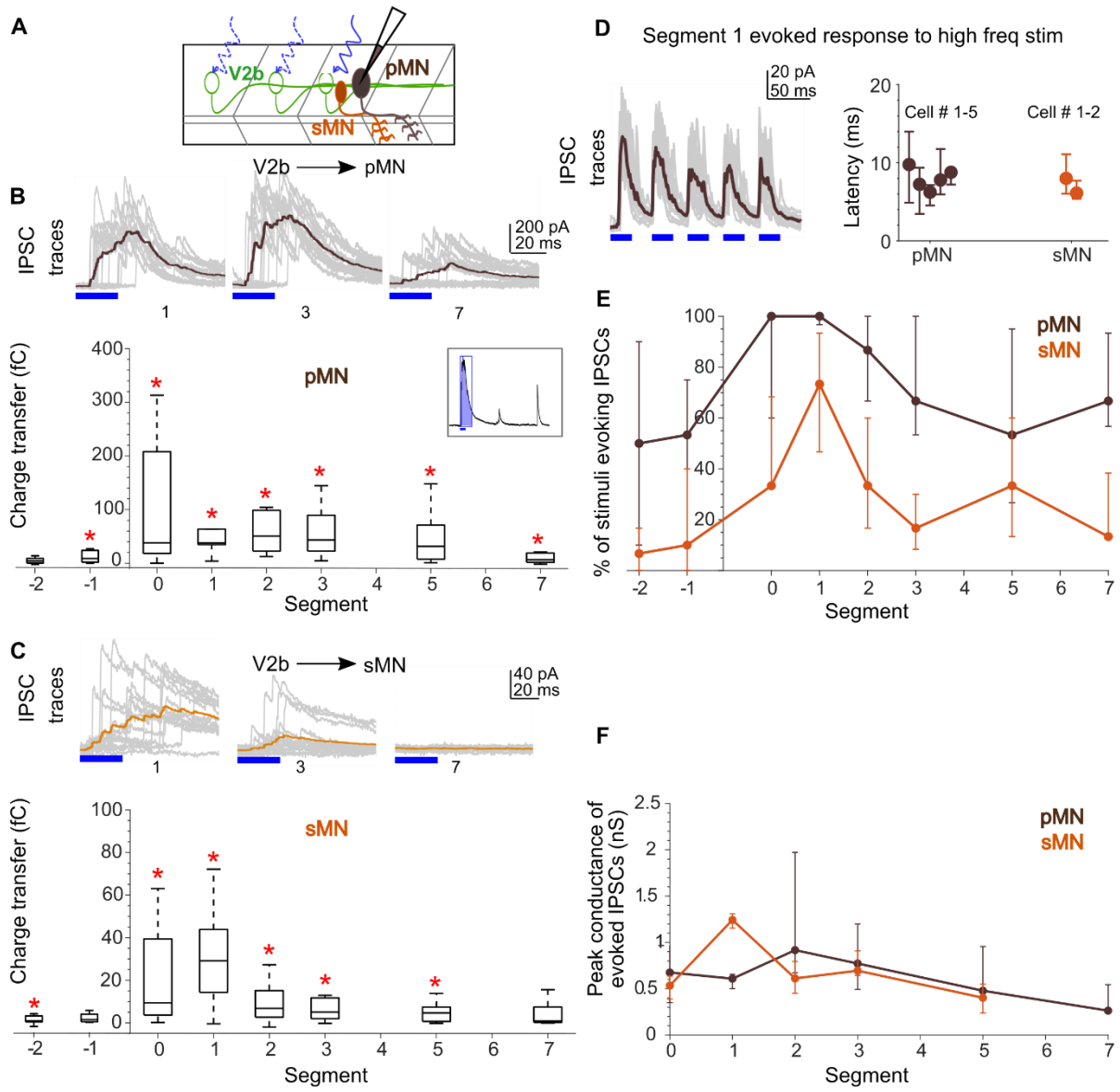

Figure 3: Motor neurons receive short- and long-range inputs from V2b neurons. A. Schematic of the experimental design showing intracellular recordings from primary (brown) and secondary (orange) motor neurons paired with optical stimulation of CatCh+ V2b neurons (green) along the rostro-caudal axis. B. Top: Representative overlay of 15 traces of IPSCs recorded in a primary motor neuron (pMN) during illumination of segments 1, 3, and 7 rostral to the recorded neuron soma. Colored trace represents mean. Duration of the optical stimulus is shown as a blue bar. Bottom: Box plots showing total charge transfer per segment (inset, illustration) recorded in primary motor neurons. In this and subsequent Figures, the box shows the median, 25th, and 75th percentile values; whiskers show +/–2.7σ. Red asterisks mark distributions that were significantly different from noise ($p < 0.01$). N = 9-25 neurons for each data point. C. Same as in B for secondary motor neurons (sMNs). N = 7-11 neurons for each data point. D. Left: Representative overlay of 10 traces of IPSCs recorded in primary motor neurons (pMNs) during a 20 Hz optical stimulus train (5 pulses, 20 ms) on segment 1. D. Right: Scatter

plot showing median latency of the first IPSC for each of the five pulses in the train stimulus for each neuron. Error bars represent 25th and 75th percentiles. Dots represent Cell # 1-5 for pMNs (brown) and 1-2 for sMNs (orange). E, F. Comparison of the percent of squares in the optical stimulus grid that evoked IPSCs (E) and the peak conductance of IPSCs (F) in primary (brown) and secondary (orange) motor neurons. Here and in subsequent Figures, circles represent median values and error bars indicate the 25th and 75th percentiles. N= 16 pMNs and 8-11 sMNs.

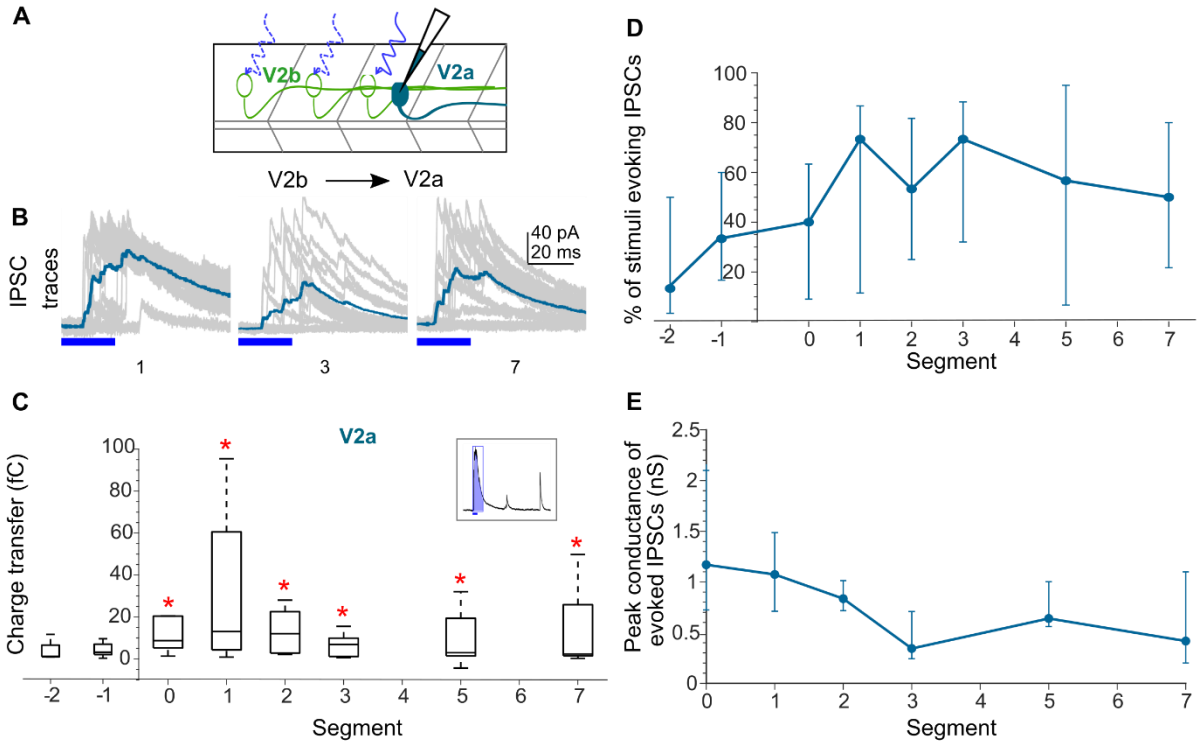

Figure 4: V2a neurons receive local and long-range inhibition from V2b neurons. A. Schematic of the experimental design showing intracellular recordings from V2a neurons (cyan) paired with optical stimulation of CatCh+ V2b neurons (green) along the rostro-caudal axis. B. Representative overlay of 15 traces of IPSCs recorded in a V2a neuron during illumination of segments 1, 3, and 7 rostral to the recorded neuron soma. Colored trace represents mean. Duration of the optical stimulus is shown as a blue bar. C. Box plot showing total charge transfer per segment (inset, illustration) recorded in V2a neurons. N = 7-10 neurons for each data point. D, E. Comparison of the percent of squares in the optical stimulus grid that evoked IPSCs (D) and the peak conductance of IPSCs (E) in V2a neurons. N=8 neurons.

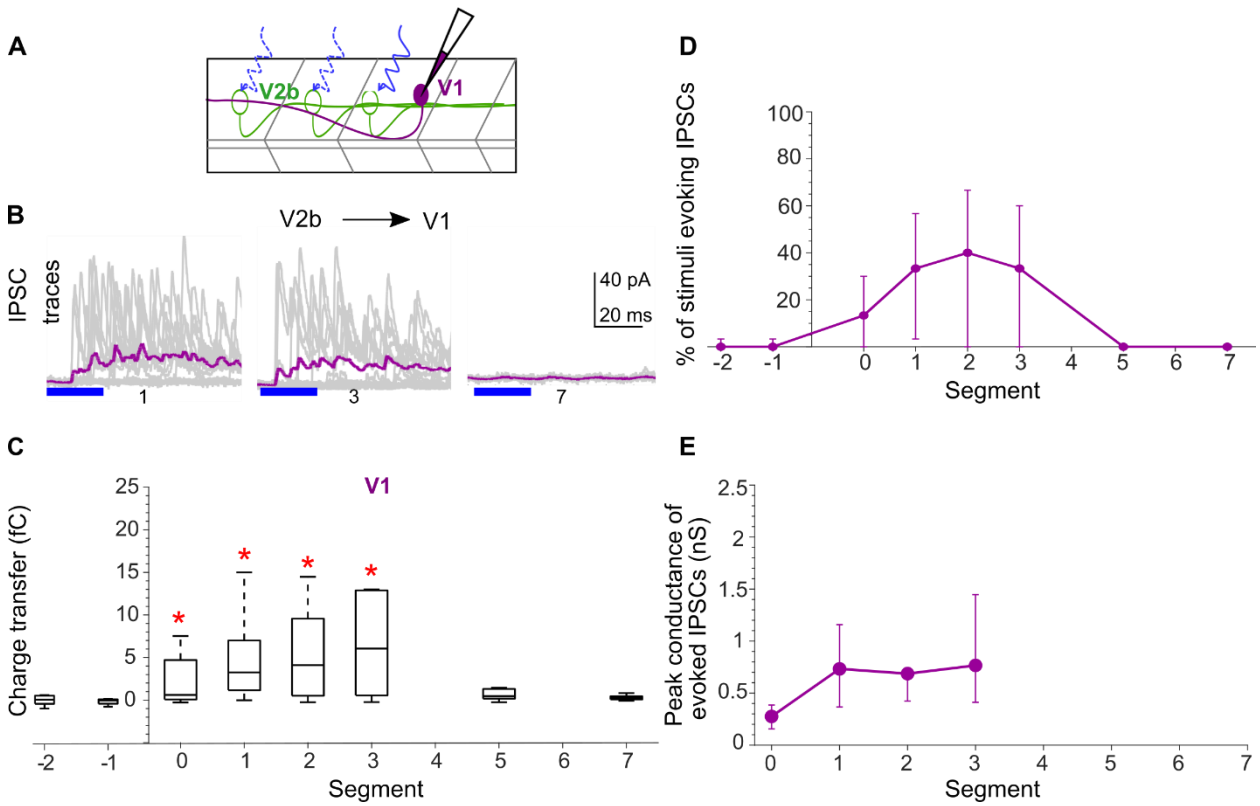

Figure 5: V1 neurons receive predominantly local V2b inhibition. A. Schematic of the experimental design showing intracellular recordings from V1 neurons (magenta) paired with optical stimulation of CatCh+ V2b neurons (green) along the rostro-caudal axis. B. Representative overlay of 15 traces of IPSCs recorded in a V2a neuron during illumination of segments 1, 3, and 7 rostral to the recorded neuron soma. Colored trace represents mean. Duration of the optical stimulus is shown as a blue bar. C. Box plot showing total charge transfer per segment (inset, illustration) recorded in V2a neurons. N = 9 neurons for each data point. D, E. Comparison of the percent of squares in the optical stimulus grid that evoked IPSCs (D) and the peak conductance of IPSCs (E) in V1 neurons. N=9 neurons.

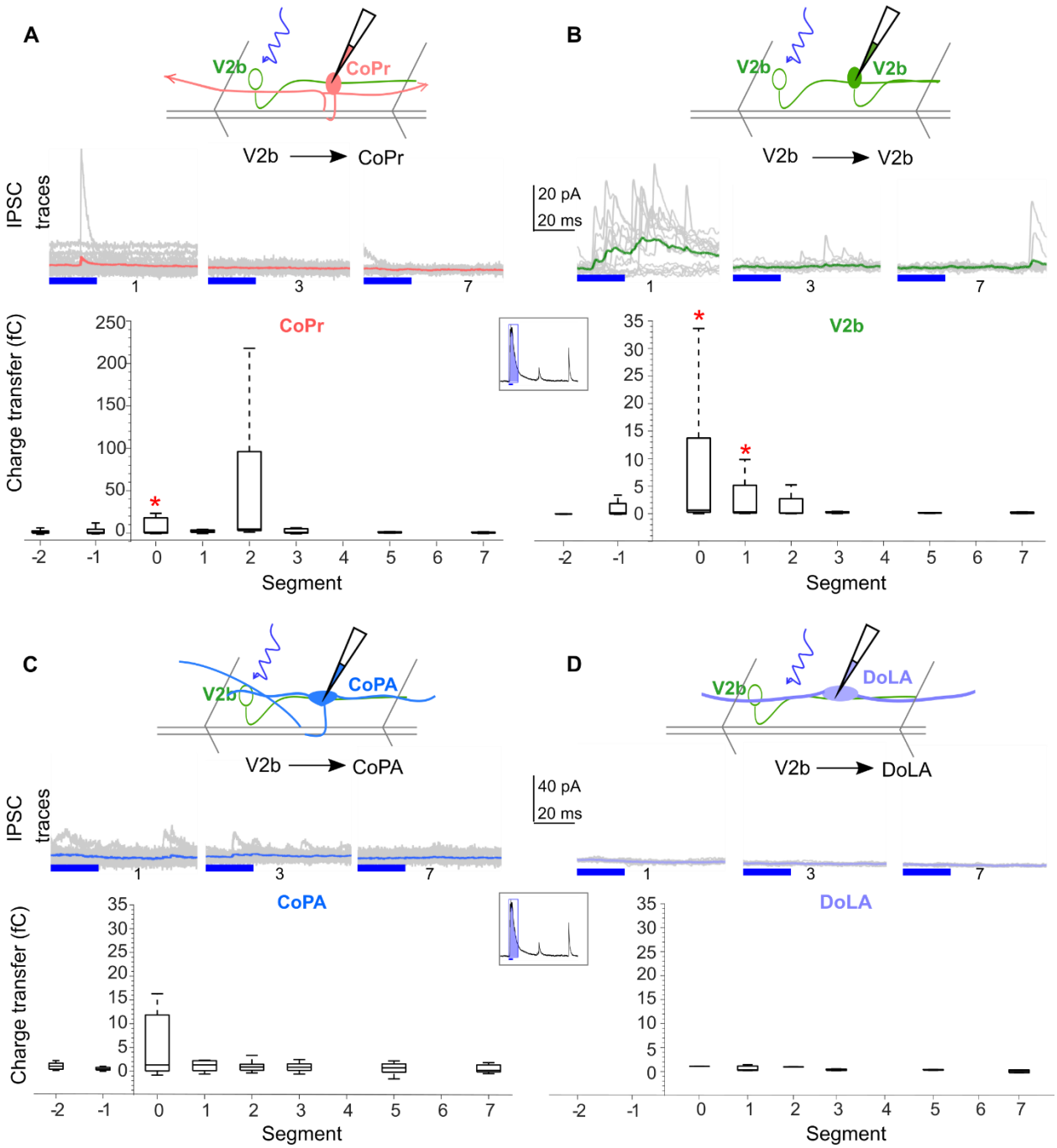

Figure 6: V2b inhibition to other spinal populations. A. V2b inhibition to Commissural Premotor neurons (CoPrs). Top: Schematic of the experimental design. Middle: Representative overlay of 15 traces of IPSCs recorded in a CoPr neuron during illumination of segments 1, 3, and 7 rostral to the recorded neuron soma. Colored trace represents mean. Duration of the optical stimulus is shown as a blue bar. Bottom: Box plot showing total charge transfer per segment (inset, illustration) recorded in V2a neurons. N = 7 neurons for each data point. B, C, D. Same as in A for V2b inhibition to other V2bs (B, N = 9 neurons), CoPA neurons (C, N = 12 neurons), and DoLA neurons (D, N = 3 neurons).

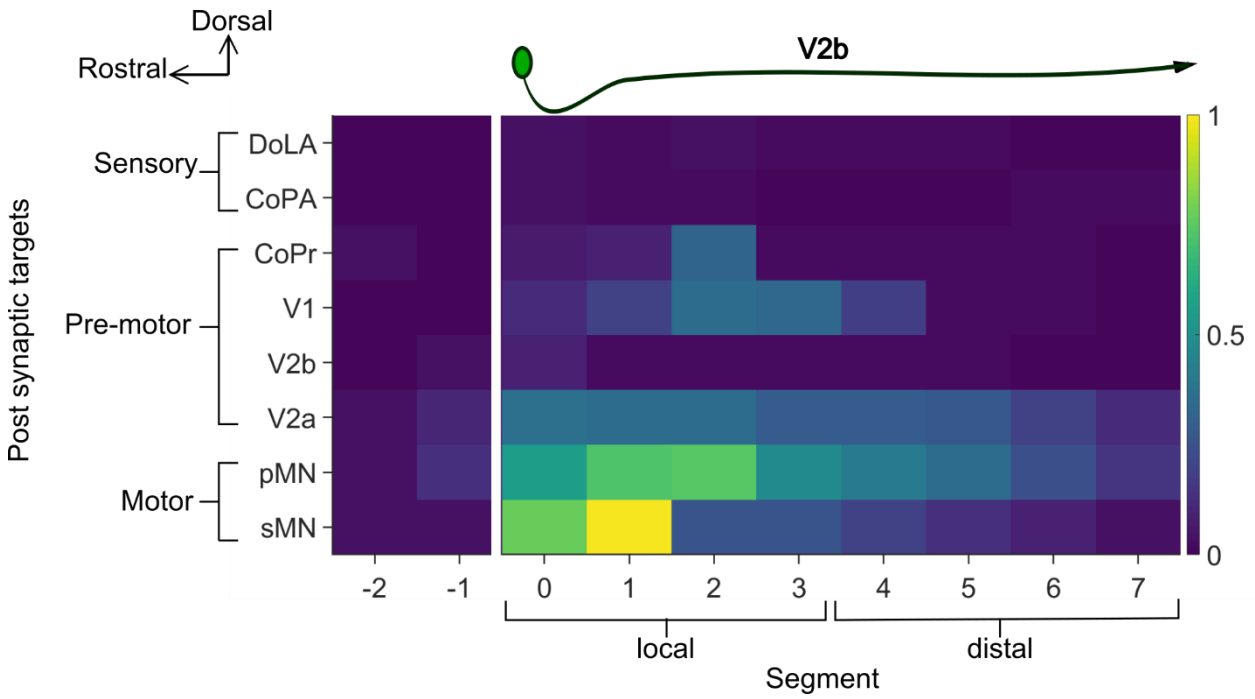

Figure 7: Summary of V2b connectivity. Heat map showing normalized charge transfer for the different post-synaptic targets along the rostro-caudal axis. The charge transfer per segment for each recorded neuronal target was normalized to its measured intrinsic neuronal conductance (inverse of R_{in}). Median values of normalized charge transfer for each target cell population are plotted. Values for Segment 4 and Segment 6 were interpolated as averages of the two neighboring segments. The resulting values are plotted on the same color scale for all target populations.

References

1. Graham Brown, T. (1914). On the nature of the fundamental activity of the nervous centres; Together with an analysis of the conditioning of rhythmic activity in progression, and a theory of the evolution of function in the nervous system. Journal of Physiology *48*, 18–46.

2. Kiehn, O. (2006). Locomotor circuits in the mammalian spinal cord. Annual Review of Neuroscience *29*, 279–306.

3. Goulding, M. (2009). Circuits controlling vertebrate locomotion: moving in a new direction. Nat Rev Neurosci *10*, 507–518.

4. Stepien, A.E., and Arber, S. (2008). Probing the Locomotor Conundrum: Descending the "V" Interneuron Ladder. Neuron *60*, 1–4.

5. Grillner, S., and Jessell, T.M. (2009). Measured motion: searching for simplicity in spinal locomotor networks. Curr Opin Neurobiol *19*, 572–586.

6. Wiggin, T.D., Peck, J.H., and Masino, M.A. (2014). Coordination of fictive motor activity in the larval zebrafish is generated by non-segmental mechanisms. PLoS ONE *9*.

7. Wolf, E., Soffe, S.R., and Roberts, A. (2009). Longitudinal neuronal organization and coordination in a simple vertebrate: A continuous, semi-quantitative computer model of the central pattern generator for swimming in young frog tadpoles. Journal of Computational Neuroscience *27*, 291–308.

8. Bonnot, A.S., Whelan, P.J., Mentis, G.Z., and O'donovan, M.J. (2002). Spatiotemporal Pattern of Motoneuron Activation in the Rostral Lumbar and the Sacral Segments during Locomotor-Like Activity in the Neonatal Mouse Spinal Cord.

9. Chevallier, S., Jan Ijspeert, A., Ryczko, D., Nagy, F., and Cabelguen, J.M. (2008). Organisation of the spinal central pattern generators for locomotion in the salamander: Biology and modelling. Brain Research Reviews *57*, 147–161.

10. Sengupta, M., Daliparthi, V., Roussel, Y., Bui, T. v., and Bagnall, M.W. (2021). Spinal V1 neurons inhibit motor targets locally and sensory targets distally. Current Biology *31*, 3820–3833.

11. Lundfald, L., Restrepo, C.E., Butt, S.J.B., Peng, C.Y., Droho, S., Endo, T., Zeilhofer, H.U., Sharma, K., and Kiehn, O. (2007). Phenotype of V2-derived interneurons and their relationship to the axon guidance molecule EphA4 in the developing mouse spinal cord. European Journal of Neuroscience *26*, 2989–3002.

12. Karunaratne, A., Hargrave, M., Poh, A., and Yamada, T. (2002). GATA proteins identify a novel ventral interneuron subclass in the developing chick spinal cord. Developmental Biology *249*, 30–43.

13. Callahan, R.A., Roberts, R., Sengupta, M., Kimura, Y., Higashijima, S.-I., and Bagnall, M.W. (2019). Spinal V2b neurons reveal a role for ipsilateral inhibition in speed control. Elife *8*.

14. Flynn, J.R., Conn, V.L., Boyle, K.A., Hughes, D.I., Watanabe, M., Velasquez, T., Goulding, M.D., Callister, R.J., and Graham, B.A. (2017). Anatomical and molecular properties of long descending propriospinal neurons in mice. Frontiers in Neuroanatomy *11*.

15. Ruder, L., Takeoka, A., and Arber, S. (2016). Long-Distance Descending Spinal Neurons Ensure Quadrupedal Locomotor Stability. Neuron *92*, 1063–1078.

16. Britz, O., Zhang, J., Grossmann, K.S., Dyck, J., Kim, J.C., Dymecki, S., Gosgnach, S., and Goulding, M. (2015). A genetically defined asymmetry underlies the inhibitory control of flexor-extensor locomotor movements. Elife *4*.

17. Zhang, J., Lanuza, G.M., Britz, O., Wang, Z., Siembab, V.C., Zhang, Y., Velasquez, T., Alvarez, F.J., Frank, E., and Goulding, M. (2014). V1 and V2b interneurons secure the alternating flexor-extensor motor activity mice require for limbed locomotion. Neuron *82*, 138–150.

18. Francius, C., Harris, A., Rucchin, V., Hendricks, T.J., Stam, F.J., Barber, M., Kurek, D., Grosveld, F.G., Pierani, A., Goulding, M., et al. (2013). Identification of Multiple Subsets of Ventral Interneurons and Differential Distribution along the Rostrocaudal Axis of the Developing Spinal Cord. PLoS ONE *8*.

19. Kimura, Y., Okamura, Y., and Higashijima, S.I. (2006). alx, a zebrafish homolog of Chx10, marks ipsilateral descending excitatory interneurons that participate in the regulation of spinal locomotor circuits. Journal of Neuroscience *26*, 5684–5697.

20. Kimura, Y., and Higashijima, S. ichi (2019). Regulation of locomotor speed and selection of active sets of neurons by V1 neurons. Nature Communications *10*.

21. Ahrens, M.B., Li, J.M., Orger, M.B., Robson, D.N., Schier, A.F., Engert, F., and Portugues, R. (2012). Brain-wide neuronal dynamics during motor adaptation in zebrafish. Nature *485*, 471–477.

22. Rothman, J.S., and Silver, R.A. (2018). Neuromatic: An integrated open-source software toolkit for acquisition, analysis and simulation of electrophysiological data. Frontiers in Neuroinformatics *12*.

23. Kawano, K., Kato, K., Sugioka, T., Kimura, Y., Tanimoto, M., and Higashijima, S. ichi (2022). Long descending commissural V0v neurons ensure coordinated swimming movements along the body axis in larval zebrafish. Scientific Reports *12*.

24. Pratt, C.A., and Jordan, L.M. (1987). Ia Inhibitory Interneurons and Renshaw Cells as Contributors to the Spinal Mechanisms of Fictive Locomotion. JOURNAL OF NEUROPHVSIOL~GY *57*, 56–71.

25. Petreanu, L., Huber, D., Sobczyk, A., and Svoboda, K. (2007). Channelrhodopsin-2-assisted circuit mapping of long-range callosal projections. Nature Neuroscience *10*, 663–668.

26. Kleinlogel, S., Feldbauer, K., Dempski, R.E., Fotis, H., Wood, P.G., Bamann, C., and Bamberg, E. (2011). Ultra light-sensitive and fast neuronal activation with the Ca 2+-permeable channelrhodopsin CatCh. Nature Neuroscience *14*, 513–518.

27. Menelaou, E., and McLean, D.L. (2012). A gradient in endogenous rhythmicity and oscillatory drive matches recruitment order in an axial motor pool. The Journal of neuroscience *32*, 10925–10939.

28. Knafo, S., and Wyart, C. (2018). Active mechanosensory feedback during locomotion in the zebrafish spinal cord. Current Opinion in Neurobiology *52*, 48–53.

29. Böhm, U.L., Prendergast, A., Djenoune, L., Figueiredo, S.N., Gomez, J., Stokes, C., Kaiser, S., Suster, M., Kawakami, K., Charpentier, M., et al. (2016). CSF-contacting neurons regulate locomotion by relaying mechanical stimuli to spinal circuits. Nature Communications *7*, 1–8.

30. Hubbard, J.M., Böhm, U.L., Prendergast, A., Tseng, P.E.B., Newman, M., Stokes, C., and Wyart, C. (2016). Intraspinal Sensory Neurons Provide Powerful Inhibition to Motor Circuits Ensuring Postural Control during Locomotion. Current Biology *26*, 2841–2853.

31. Menelaou, E., and McLean, D.L. (2019). Hierarchical control of locomotion by distinct types of spinal V2a interneurons in zebrafish. Nature Communications *10*.

32. Kimura, Y., Satou, C., Fujioka, S., Shoji, W., Umeda, K., Ishizuka, T., Yawo, H., and Higashijima, S.I. (2013). Hindbrain V2a neurons in the excitation of spinal locomotor circuits during zebrafish swimming. Current Biology *23*, 843–849.

33. Ampatzis, K., Song, J., Ausborn, J., and ElManira, A. (2014). Separate Microcircuit Modules of Distinct V2a Interneurons and Motoneurons Control the Speed of Locomotion. Neuron *83*, 934–943.

34. Song, J., Dahlberg, E., and el Manira, A. (2018). V2a interneuron diversity tailors spinal circuit organization to control the vigor of locomotor movements. Nature Communications *9*.

35. Crone, S.A., Quinlan, K.A., Zagoraiou, L., Droho, S., Restrepo, C.E., Lundfald, L., Endo, T., Setlak, J., Jessell, T.M., Kiehn, O., et al. (2008). Genetic Ablation of V2a Ipsilateral Interneurons Disrupts Left-Right Locomotor Coordination in Mammalian Spinal Cord. Neuron *60*, 70–83.

36. Dougherty, K.J., Zagoraiou, L., Satoh, D., Rozani, I., Doobar, S., Arber, S., Jessell, T.M., and Kiehn, O. (2013). Locomotor Rhythm Generation Linked to the Output of Spinal Shox2 Excitatory Interneurons. Neuron *80*, 920–933.

37. Higashijima, S.I., Masino, M.A., Mandel, G., and Fetcho, J.R. (2004). Engrailed-1 expression marks a primitive class of inhibitory spinal interneuron. Journal of Neuroscience *24*, 5827–5839.

38. Gosgnach, S., Lanuza, G.M., Butt, S.J.B., Saueressig, H., Zhang, Y., Velasquez, T., Riethmacher, D., Callaway, E.M., Kiehn, O., and Goulding, M. (2006). V1 spinal neurons regulate the speed of vertebrate locomotor outputs. Nature *440*, 215–219.

39. Li, W.C., Higashijima, S.I., Parry, D.M., Roberts, A., and Soffe, S.R. (2004). Primitive roles for inhibitory interneurons in developing frog spinal cord. Journal of Neuroscience *24*, 5840–5848.

40. Jankowska, E. (1992). Interneuronal Relay in Spinal Pathways from proprioceptors. Progress in Neurobiology *38*, 335–378.

41. Wilson, J.M., Blagovechtchenski, E., and Brownstone, R.M. (2010). Genetically defined inhibitory neurons in the mouse spinal cord dorsal horn: A possible source of rhythmic inhibition of motoneurons during fictive locomotion. Journal of Neuroscience *30*, 1137–1148.

42. Baldissera, F., Cavallari, P., Fournier, E., Pierrot-Deseilligny, E., and Shindo, M. (1987). Evidence for mutual inhibition of opposite Ia interneurones in the human upper limb. Exp Brain Res *66*, 106–114.

43. Alvarez, F.J., Jonas, P.C., Sapir, T., Hartley, R., Berrocal, M.C., Geiman, E.J., Todd, A.J., and Goulding, M. (2005). Postnatal phenotype and localization of spinal cord V1 derived interneurons. Journal of Comparative Neurology *493*, 177–192.

44. Talpalar, A.E., Bouvier, J., Borgius, L., Fortin, G., Pierani, A., and Kiehn, O. (2013). Dual-mode operation of neuronal networks involved in left-right alternation. Nature *500*, 85–88.

45. Danner, S.M., Zhang, H., Shevtsova, N.A., Borowska-Fielding, J., Deska-Gauthier, D., Rybak, I.A., and Zhang, Y. (2019). Spinal V3 Interneurons and Left–Right Coordination in Mammalian Locomotion. Frontiers in Cellular Neuroscience *13*.

46. Haque, F., Rancic, V., Zhang, W., Clugston, R., Ballanyi, K., and Gosgnach, S. (2018). WT1-expHaque, F., Rancic, V., Zhang, W., Clugston, R., Ballanyi, K., & Gosgnach, S. (2018). WT1-expressing interneurons regulate left–right alternation during Mammalian locomotor activity. Journal of Neuroscience, 38(25), 5666–5676. https://doi.org/10.152. Journal of Neuroscience *38*, 5666–5676.

47. Böhm, U.L., Kimura, Y., Kawashima, T., Ahrens, M.B., Higashijima, S., Engert, F., and Cohen, A.E. (2022). Voltage imaging identifies spinal circuits that modulate locomotor adaptation in zebrafish. Neuron.

48. Wiggin, T.D., Montgomery, J.E., Brunick, A.J., Peck, J.H., and Masino, M.A. (2022). V3 Interneurons Are Active and Recruit Spinal Motor Neurons during In Vivo Fictive Swimming in Larval Zebrafish. eNeuro *9*.

49. Kishore, S., Cadoff, E.B., Agha, M.A., and Mclean, D.L. (2020). Orderly compartmental mapping of premotor inhibition in the developing zebrafish spinal cord. Science (1979) *370*, 431–436.

50. Satou, C., Sugioka, T., Uemura, Y., Shimazaki, T., Zmarz, P., Kimura, Y., and Higashijima, S. ichi (2020). Functional Diversity of Glycinergic Commissural Inhibitory Neurons in Larval Zebrafish. Cell Reports *30*, 3036-3050.e4.

51. Andersson, L.S., Larhammar, M., Memic, F., Wootz, H., Schwochow, D., Rubin, C.J., Patra, K., Arnason, T., Wellbring, L., Hjälm, G., et al. (2012). Mutations in DMRT3 affect locomotion in horses and spinal circuit function in mice. Nature *488*, 642–646.

52. Satou, C., Kimura, Y., and Higashijima, S. ichi (2012). Generation of multiple classes of V0 neurons in Zebrafish spinal cord: Progenitor heterogeneity and temporal control of neuronal diversity. Journal of Neuroscience *32*, 1771–1783.

53. Knogler, L.D., and Drapeau, P. (2014). Sensory gating of an embryonic zebrafish interneuron during spontaneous motor behaviors. Frontiers in Neural Circuits *8*.

54. McCrea, D.A., and Rybak, I.A. (2008). Organization of mammalian locomotor rhythm and pattern generation. Brain Research Reviews *57*, 134–146.

55. Berg, R.W., Alaburda, A., and Hounsgaard, J. (2007). Balanced Inhibition and Excitation Drive Spike Activity in Spinal Half-Centers. Science (1979) *315*, 390 LP – 393.

56. Kishore, S., Bagnall, M.W., and McLean, D.L. (2014). Systematic shifts in the balance of excitation and inhibition coordinate the activity of axial motor pools at different speeds of locomotion. J Neurosci *34*, 14046–14054.

57. Isaacson, J.S., and Scanziani, M. (2011). How inhibition shapes cortical activity. Neuron *72*, 231–243.

58. Johnson, M.D., Hyngstrom, A.S., Manuel, M., and Heckman, C.J. (2012). Push-pull control of motor output. Journal of Neuroscience *32*, 4592–4599.

59. Vestergaard, M., and Berg, R.W. (2015). Divisive gain modulation of motoneurons by inhibition optimizes muscular control. Journal of Neuroscience *35*, 3711–3723.

60. Juvin, L., Simmers, J., and Morin, D. (2005). Propriospinal circuitry underlying interlimb coordination in mammalian quadrupedal locomotion. Journal of Neuroscience *25*, 6025–6035.

61. McLean, D.L., Masino, M.A., Koh, I.Y.Y., Lindquist, W.B., and Fetcho, J.R. (2008). Continuous shifts in the active set of spinal interneurons during changes in locomotor speed. Nature Neuroscience *11*, 1419–1429.

62. Danner, S.M., Shevtsova, N.A., Frigon, A., and Rybak, I.A. (2017). Computational modeling of spinal circuits controlling limb coordination and gaits in quadrupeds.

63. Laliberte, A.M., Goltash, S., Lalonde, N.R., and Bui, T.V. (2019). Propriospinal Neurons: Essential Elements of Locomotor Control in the Intact and Possibly the Injured Spinal Cord. Frontiers in Cellular Neuroscience *13*.

64. Jung, H., Baek, M., D'Elia, K.P., Boisvert, C., Currie, P.D., Tay, B.H., Venkatesh, B., Brown, S.M., Heguy, A., Schoppik, D., et al. (2018). The Ancient Origins of Neural Substrates for Land Walking. Cell *172*, 667-682.e15.

65. Ko, H.-Y. (2019). Development and Functional Anatomy of the Spine and Spinal Cord. In Management and Rehabilitation of Spinal Cord Injuries (Springer Singapore), pp. 13–48.

66. Jung, H., and Dasen, J.S. (2015). Evolution of patterning systems and circuit elements for locomotion. Developmental Cell *32*, 408–422.

67. Shevtsova, N.A., and Rybak, I.A. (2016). Organization of flexor–extensor interactions in the mammalian spinal cord: insights from computational modelling. Journal of Physiology *594*, 6117–6131.

68. Machado, T.A., Pnevmatikakis, E., Paninski, L., Jessell, T.M., and Miri, A. (2015). Primacy of Flexor Locomotor Pattern Revealed by Ancestral Reversion of Motor Neuron Identity. Cell *162*, 338–350.